Available online at www.sciencedirect.com
ScienceDirect
Journal of Catalysis 250 (2007) 274–282
JOURNAL OF CATALYSIS
www.elsevier.com/locate/jcat

Copper(II) ion exchanged AlSBA-15: A versatile catalyst for intermolecular hydroamination of terminal alkynes with aromatic amines

Ganapati V. Shanbhag, Trissa Joseph, S.B. Halligudi *

Inorganic Chemistry and Catalysis Division, National Chemical Laboratory, Pune 411008, India

Received 25 April 2007; revised 7 June 2007; accepted 7 June 2007

Available online 31 July 2007

Abstract

The hydroamination reaction offers a very attractive route for the synthesis of alkylated amines and their derivatives with no byproduct formation. AlSBA-15 was synthesized by isomorphous substitution of aluminum into the framework of SBA-15, which induces the Brönsted acid sites, and these were exchanged with metal ions such as Cu^{2+}, Zn^{2+}, and Pd^{2+}. The catalysts were characterized by XRD, N_2-sorption, SEM, TEM, acidity measurements by FT-IR pyridine adsorption, H_2-TPR, ^{27}Al MAS NMR, and ^{29}Si MAS NMR. Hydroamination of phenylacetylene (PhAc) with 2,4-xylidine has been used as a test reaction, which gave *N*-(1-phenylethylidene)-2,4-dimethylaniline with no byproduct formation. CuAlSBA-15 and CuAlMCM-41 showed around three times greater activity in hydroamination of PhAc compared with Cu-clay and Cu-beta, due to the moderate Lewis acidity of Cu^{2+} present in mesoporous supports. The performance of the CuAlSBA-15 was also determined with different alkynes and amines to evaluate the catalyst's general applicability in hydroamination reactions.

Keywords: Mesoporous; Copper catalyst; AlSBA-15; Heterogeneous; Ion exchange; Hydroamination; Addition; Alkyne; Amine

1. Introduction

The catalytic hydroamination of alkenes and alkynes with amines is the most desirable transformation leading to C–N bond formation. It offers a direct route to the synthesis of nitrogen-containing organics, such as alkylated amines, enamines, imines, and *N*-heterocycles, which are the building blocks for wide variety of compounds in the area of natural products, pharmaceuticals, dyes, fine chemicals, polymers, and surfactants [1]. The 100% atom economy makes hydroamination more attractive, because no byproducts, such as salts or water, are produced. Condensation of ketones with amines is the conventional method for preparing enamines and imines, but this reaction produces water as a byproduct, which makes it less atom-efficient and limits its use in certain reactions [2].

The earliest report dates back to 1939, when Loritsch and Vogt used mercuric oxide and boron fluoride in stoichiometric amounts for hydroamination of alkynes with anilines [3]. Since then, various approaches using homogeneous catalysts, such as transition metal salts, lanthanide and actinide complexes, and transition metal complexes, have been studied for this seemingly simple but challenging transformation [4–10]. But homogeneous methods suffer from their tedious workup procedure and low catalyst recyclability. There is a need to develop efficient, sustainable, recyclable, and eco-friendly solid catalysts for hydroamination reactions. Compared with homogeneous catalysts, only a handful of heterogeneous catalysts have been reported to date. Penzien et al. developed metal-exchanged zeolites for alkyne hydroamination, which favors Markovnikov addition products [11–14]. But zeolite-based catalysts normally show low activity toward bulkier substrates due to pore size restrictions. Pd complex immobilized on silica has been reported for intramolecular cyclization of amino-alkynes [15]. Ionic liquids supported on diatomic earth and silver-exchanged tungstophosphoric acid also have been reported for heterogeneous hydroamination of terminal alkynes [16,17].

Mesoporous materials such as MCM-41 and SBA-15 have advantages over zeolites due to their larger pore size and higher surface area. The isomorphous substitution of aluminum into the mesoporous framework of MCM-41 and SBA-15 induces Brönsted acidity and can act as ion-exchange sites [18]. Meso-

* Corresponding author. Fax: +91 20 25902633.
E-mail address: sb.halligudi@ncl.res.in (S.B. Halligudi).

0021-9517/$ – see front matter
doi:10.1016/j.jcat.2007.06.007

porous solids such as AlSBA-15 and AlMCM-41 have an ordered porous structure, and the active components tailored in their nano-ordered spaces will improve their catalytic performance. Transition metal ions can be introduced by ion exchange in different states and coordination on their surfaces as well as inside the pores. Metal cations located at different ion-exchange positions will have distinct stability as well as reactivity. Over the past few decades, several catalytic studies have been made using transition metal ion-exchanged porous solids and clays [19–24]. Recently, CuMCM-41 was reported for 1-butene isomerization and hydroxylation of phenol [25,26]. Very few reports on CuAlSBA-15 are available in the literature. In one such report, aluminum has been incorporated in the framework of SiSBA-15 by a postsynthesis method and Cu^{2+} ions were exchanged to evaluate the ion-exchange property of AlSBA-15 [27]. In our earlier studies, we have reported metal-exchanged montmorillonite clay for intermolecular hydroamination of terminal alkynes with aromatic amines [28–30]. The present study deals with the synthesis, characterization, and applications of metal ion-exchanged catalysts such as CuAlSBA-15 in the synthesis of imines from the hydroamination of alkynes with aromatic amines.

2. Experimental

2.1. Materials

Amines and solvents were purchased from Merck India Ltd; alkynes and montmorillonite K-10 were procured from Aldrich, USA. Zeolite H-beta was obtained from CPP, NCL, Pune. All of the chemicals were of research grade and were used after drying following standard procedures.

2.2. Catalyst preparation

2.2.1. Synthesis of SBA-15

A detailed procedure for synthesizing mesoporous silica SBA-15 was reported by Zhao et al. [31]. In a typical synthesis, 4 g of amphiphilic triblock copolymer, poly(ethylene glycol)-block-poly(propylene glycol)-block-poly(ethylene glycol) (average molecular weight, 5800), was dispersed in 30 g of water, and 120 g of 2 M HCl solution was added while stirring. This was followed by the addition of 8 g of tetraethyl orthosilicate to the homogeneous solution with stirring. This gel mixture was continuously stirred at 40 °C for 24 h and finally crystallized in a Teflon-lined autoclave at 100 °C for 2 days. After crystallization, the solid product was filtered, washed with distilled water, and dried in air at room temperature. The material was calcined in static air at 550 °C for 24 h to decompose the triblock copolymer and obtain a white powder (SBA-15).

2.2.2. Synthesis of AlSBA-15

SBA-15 was used as the parent material to synthesize AlSBA-15 via a postsynthesis route similar to that reported elsewhere [27]. Silica SBA-15 (1 g) was combined with 25 ml of dry ethanol containing various amounts of $AlCl_3$ with magnetic stirring at 80 °C for 10 h. The solid material was then filtered, washed vigorously with dry ethanol, and dried at room temperature in air. It was calcined in static air at 550 °C for 5 h. AlMCM-41 was synthesized as we described previously [32].

2.2.3. Synthesis of CuAlSBA-15

A known amount of AlSBA-15 (1 g) was stirred with 0.03 M cupric acetate solution prepared in water (20 ml) at 80 °C for 6 h and then cooled to room temperature. Then the exchanged AlSBA-15 was filtered, washed repeatedly with distilled water, and dried in air. This procedure was repeated to ensure maximum copper exchange. Then it was dried at 120 °C for 12 h and calcined at 500 °C for 5 h (room temperature to 500 °C; ramp rate, 4 °C min^{-1}; 4 h at 500 °C). This procedure was applied to all of the other catalyst preparations. Similarly, all other metal-exchanged catalysts with different supports were prepared by exchanging with the predetermined stock solutions of the corresponding metal acetate by following the above procedure except for La and Fe, for which $LaCl_3$ and $FeCl_3$ solutions were used. For a comparative study with the exchanged catalysts, 2 wt% copper was loaded over SBA-15 (hereinafter CuO/SBA-15) by the wet impregnation method. SBA-15 was added to aqueous copper acetate solution, stirred well for 10 h, evaporated to dryness, and calcined at 500 °C. These materials are designated AlSBA-15-(X) and MAlSBA-15 (X), where M is the exchanged metal ion and X is the Si/Al ratio of the chemical stoichiometric composition taken in the postsynthesis mixtures.

2.3. Characterization

2.3.1. Structure and texture characterization

Low-angle X-ray diffraction patterns of mesoporous samples were collected on a Philips X' Pert Pro 3040/60 diffractometer using Cu$K\alpha$ radiation ($l = 1.5418$ Å), a nickel filter, and an X'celerator as a detector, using the real time multiple strip (RTMS) detection technique. XRD patterns were collected in the range of $2\theta = 0.5°$–$5°$.

The specific surface areas of the catalysts were measured by N_2 physisorption at liquid nitrogen temperature with an Omnisorb 100 CX (Coulter). Samples were dried at 300 °C in a dynamic vacuum for 2 h before the N_2 physisorption measurements. The specific surface area was determined using the standard BET method on the basis of adsorption data. The pore size distributions were calculated from both adsorption and desorption branches of the isotherms using the BJH method and the corrected Kelvin equation [33]. Pore volume values were determined using the t-plot method of De Boer.

TEM photographs were obtained with a JEOL Model 1200 EX microscope operated at an accelerating voltage of 120 kV. Samples were prepared by placing droplets of a suspension of the sample in isopropanol on a polymer microgrid supported on a Cu grid for TEM measurements. SEM was used to characterize the surface morphology with a Leica stereoscan Cambridge 440 Microscope (UK) with a Kevex model EDAX system.

2.3.2. Elemental analysis

The Si/Al ratios of the catalyst samples were determined by XRF spectroscopy using a Shimadzu XRF-1700 sequen-

tial XRF spectrometer. The amount of exchanged metal ions on the supports was determined using an atomic absorption spectrophotometer (AAS-Hitachi Model Z-8000) except for Pd (determined by ICP-OES) by following standard procedures.

2.3.3. NMR measurements

Magic-angle spinning (MAS) NMR spectra were recorded on a BRUKER DSX300 spectrometer at 7.05 T (resonance frequency, 59.63 MHz; ^{29}Si: rotor speed, 4000 Hz; number of scans, 5275 and 78.19 MHz; ^{27}Al: rotor speed, 6000 Hz; number of scans, 2800). External $Al(H_2O)_6^{3+}$ was used as a reference.

2.3.4. FTIR pyridine adsorption measurements

The nature of the acid sites (Brönsted and Lewis) of the catalyst samples with different loadings were characterized by in situ Fourier transform infrared (FTIR) spectroscopy with chemisorbed pyridine in drift mode on an FTIR-8300 Shimadzu SSU-8000 instrument with 4 cm^{-1} resolution and averaged over 500 scans. These studies were performed by heating precalcined powder samples in situ from room temperature to 400 °C at a heating rate of 5 °C min^{-1} in a flowing stream (40 ml min^{-1}) of pure N_2. The samples were kept at 400 °C for 3 h and then cooled to 100 °C, after which pyridine vapors (20 μl) were introduced under N_2 flow. The IR spectra were recorded with 4 cm^{-1} resolution and 500 scans after the sample was degassed at 200 °C for 30 min.

2.3.5. H_2-TPR

The reducibility of the calcined copper catalysts was measured by TPR method using a Micromeritics AutoChem 2910 instrument. About 300 mg of the catalyst was mounted in a quartz tube and calcined in argon flow at 500 °C for 1 h (temperature-programmed rate, 10 °C min^{-1}) with the aim of removing the substances that were physisorbed. It was then cooled to ambient temperature in argon before the reduction by a mixing gas of hydrogen and helium (5% H_2 in volume percentage). In the H_2-TPR analysis, the heating rate was 10 °C min^{-1} and the gas flow was 10 ml min^{-1}. The cold trap consisted of liquid nitrogen and 2-propanol. The hydrogen consumed during the reduction was determined by a thermal conductivity detector.

2.3.6. Catalyst testing

In a typical reaction, the reaction mixture consisting of 0.59 g of phenyl acetylene (PhAc), 1.41 g of 2,4-xylidine, 2 ml of toluene, and 0.1 g of catalyst (activated at 300 °C for 4 h before use) was placed in a 50-ml round-bottomed flask in an oil bath and refluxed at 110 °C under N_2 atmosphere. Samples were withdrawn at regular intervals and analyzed using a Shimadzu 14B gas chromatograph equipped with a flame ionization detector using a capillary column. Reactions at temperatures above the boiling point of toluene or substrate were performed in a 50-ml Parr autoclave. To determine the general applicability of the catalyst, the reactions were carried out with different alkynes and aromatic amines. Conversion of PhAc was expressed in mol%. To determine the authenticity of the product, the reaction mixture was cooled and filtered to remove the catalyst, and the solvent was removed by distillation. The mixture was dried in vacuo and purified by column chromatography on silica gel (petroleum ether/ethyl acetate, 200/1). *N*-(1-phenylethylidene)-2,4-dimethylaniline. Light brown oil: ^{1}H NMR ($CDCl_3$, 200 MHz): $\delta = 7.93$–8.02 (m, 2H), 7.43–7.57 (m, 3H), 7.02 (d, 1H), 6.86 (m, 1H), 6.56 (m, 1H), 2.31 (s, 3H), 2.16 (s, 3H), 2.06 (s, 3H). FTIR (neat, cm^{-1}): 3020, 2951, 1639, 1209, 847, 764, 631. GCMS m/z (relative intensity): 223 (54) [M^+], 208 (100), 193 (35), 146 (12), 103 (35), 77 (67), 51 (25).

Hydration of alkyne with water (with the addition of H–OH over the triple bond and subsequent rearrangement giving a ketone) is the side reaction that may occur in the presence of an acid catalyst at a faster rate than hydroamination. Hence the chemicals and the reaction setup must be free of water to avoid a hydration reaction.

3. Results and discussion

3.1. Physicochemical characterization

3.1.1. X-ray diffraction

Well-defined XRD patterns were obtained for all samples and were similar to those recorded for SBA-15 materials as described by Zhao et al. [31]. XRD patterns of calcined SBA-15, Al-SBA-15 (10), and CuAlSBA-15 (10) materials with different Si/Al ratios (see Figs. 1a, 1b, and 1c, respectively) consisted of three well-resolved peaks in the 2θ range of 0.8°–1.8° corresponding to the (100), (110), and (200) reflections associated with *p6mm* hexagonal symmetry in the materials. It is noteworthy that no obvious change was seen after the isomorphous substitution of Al into the framework of siliceous SBA-15 by the postsynthesis method, implying that the hexagonal mesoporous structure was well preserved. The XRD profile of the samples demonstrated no other phases or amorphous matter. In addition, the XRD pattern of CuMCM-41 (15) (Fig. 1d) shows the appearance of the (100), (110), and (200) reflections in lower 2θ region, demonstrating the well-ordered nature of phases in the CuAlMCM-41.

3.1.2. Nitrogen sorption studies

Textural properties of porous solids are typically obtained from low-temperature (−196 °C) nitrogen adsorption isotherms, which allow computation of the specific surface area, specific pore volume, and mesopore size distribution. The nitrogen adsorption–desorption isotherms of AlSBA-15 (10) and CuSBA-15 samples of different Si/Al ratios are shown in Fig. 2, and the textural properties of all samples are presented in Table 1. All isotherms were of type IV, as defined by IUPAC, and exhibited an H1-type broad hysteresis loop typical of large-pore mesoporous solids. As the relative pressure increased ($p/p_0 > 0.6$), all isotherms exhibited a sharp step characteristic of capillary condensation of nitrogen within uniform mesopores, where the p/p_0 position of the inflection point is correlated with the diameter of the mesopore. The pore size

Table 1
Structural characteristics of different catalysts and their catalytic activities

Catalyst	Si/Al (XRF)	Surface area BET (m^2/g^{-1})	Pore volume (cm^3/g)	Average pore diameter	Copper conc. (mmol/g)	PhAc convn.[a] (mol%)	TOF[b]
SBA-15	∞	745	1.03	66.6	–	1.2	–
AlSBA-15 (10)	17	685	1.31	76.7	–	2.0	–
AlSBA-15 (20)	26	730	1.16	66.3	–	1.8	–
AlSBA-15 (30)	36	720	0.99	63.5	–	1.5	–
AlSBA-15 (40)	43	620	0.98	63.4	–	1.3	–
AlMCM-41 (15)	15	962	0.80	33.6	–	2.1	–
H-beta	15	530	0.28	–	–	1.5	–
Clay	–	230	–	–	–	1.2	–
CuAlSBA-15 (10)	–	664	1.09	67.9	0.21	48	22
CuAlSBA-15 (20)	–	685	0.95	65.8	0.15	37	24
CuAlSBA-15 (30)	–	603	0.98	67.7	0.11	27	25
CuAlSBA-15 (40)	–	652	1.1	67.6	0.09	21	23
CuO/SBA-15	–	685	0.95	66.0	0.31	8	3
CuAlMCM-41 (15)	–	820	0.72	33.1	0.26	52	21
Cu-clay	–	208	–	–	0.22	28	9
Cu-beta (15)	–	480	–	–	0.25	31	7
$Cu(CF_3SO_3)_2$	–	–	–	–	–	37	17
CuO	–	–	–	–	–	0	–

[a] Conditions: temperature = 110 °C, 2,4-xylidine to PhAc mole ratio = 2, catalyst wt = 0.15 g, total reactants wt = 2 g, time = 6 h.
[b] TOF = mole of PhAc converted per mole copper per hour.

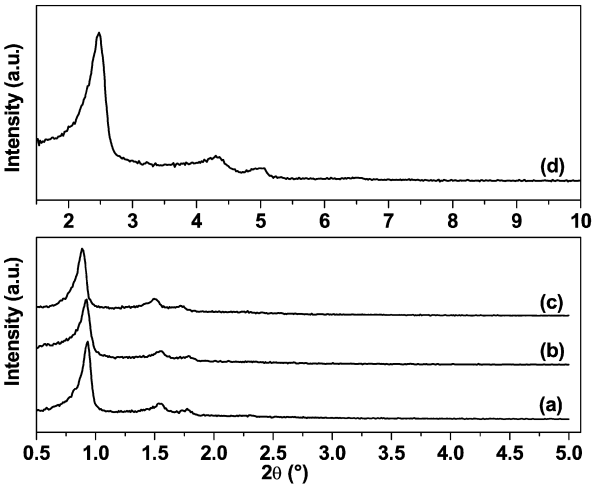

Fig. 1. Low angle XRD patterns of (a) SBA-15, (b) AlSBA-15, (c) CuAlSBA-15 (10), (d) CuAlMCM-41.

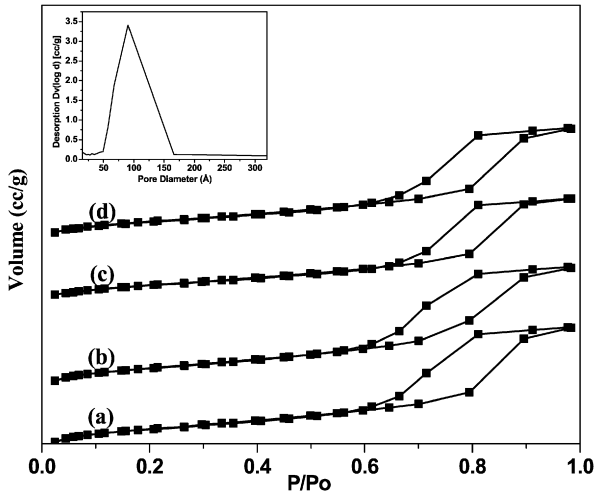

Fig. 2. N_2 adsorption and desorption isotherms of nitrogen on samples: (a) AlSBA-15 (10), (b) CuAlSBA-15 (10), (c) CuAlSBA-15 (30), (d) CuAlSBA-15 (40); Inset picture: pore size distribution of CuAlSBA-15 (10).

distribution was calculated from the Kelvin equation and is presented as a BJH plot (Fig. 2, inset) exhibiting a narrow pore size distribution with an average mesopore size of 91 Å and a high surface area ABJH of 685 m^2/g. The N_2 adsorption isotherms of all CuAlSBA-15 materials were quite similar to the isotherm of AlSBA-15. The overall N_2 adsorption decreased depending on the aluminum loading, although no particular trend was observed. The calculated BET specific surface areas, total pore volume, and average mesopore parameters based on BJH plots are listed in Table 1. Low alumination of SBA-15 did not affect the original pore structure of the parent SBA-15, but the surface area decreased slightly with increased aluminum loadings. Further modification of AlSBA-15 materials with copper exchange and calcination reduces the surface areas slightly, as expected. CuAlMCM-41 (15) had a higher surface area but lower average pore diameter than CuAlSBA-15 (10) (820 vs 664 m^2/g and 33.1 vs 67.9 Å, respectively. The surface areas of Cu-beta (480 m^2/g) and Cu-clay (207 m^2/g) were lower than that of CuAlSBA-15.

3.1.3. Microscopic analysis

SEM images of CuAlSBA-15 (Fig. 4) reveal that the micromorphology remained the same, with rope-like structures, even after modification of SBA-15 with postsynthesis Al incorporation and Cu^{2+} exchange. TEM measurements were carried out to study the morphology of the AlSBA-15 and CuAlSBA-15 catalysts (Fig. 3). TEM images of these catalysts demonstrated retention of the periodic structure of parent SBA-15 precursor (not shown), confirming that the hexagonally arranged mesopores of SBA-15 were retained after modification with aluminum and copper.

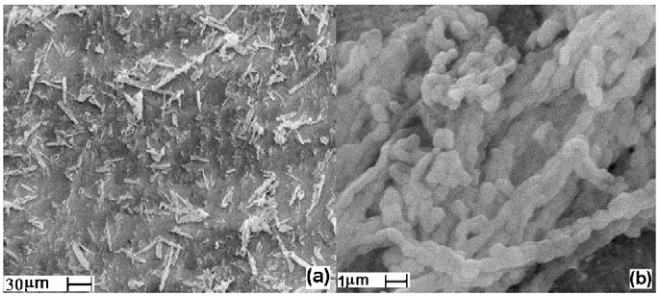

Fig. 3. SEM photographs of (a) and (b) CuAlSBA-15.

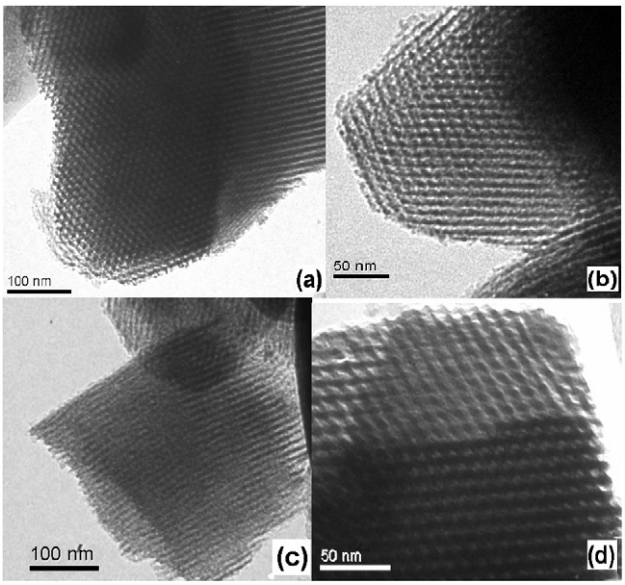

Fig. 4. TEM photographs of (a) and (b) AlSBA-15 (10), (c) and (d) CuAlSBA-15.

3.1.4. Nuclear magnetic resonance

Solid-state ^{27}Al MAS NMR (Fig. 5) was used to investigate the local environment of aluminum species. The sharp peak observed at 53 ppm, corresponding to tetrahedrally coordinated framework aluminum in which Al is bound covalently to four Si atoms via oxygen bridges, indicates that most of the aluminum was incorporated into the framework. The peak at 0 ppm can be attributed to distorted or octahedrally coordinated aluminum species in extra-framework positions. In addition, the presence of distorted tetrahedral or five-coordinated aluminum cannot be discarded due to the low-intensity signals observed at around 30 ppm [34]. Compared with the ZnAlSBA-15 (10) sample, CuAlSBA-15 (10) had a larger line width and lower-intensity ^{27}Al NMR signal at 53 ppm, indicating the presence of paramagnetic Cu^{2+} ions near the aluminum sites in AlSBA-15. The intensity of octahedral Al signal at 0 ppm was reduced after metal ion exchange, possibly due to the removal of extra-framework aluminum during the ion exchange of AlSBA-15 with the metal acetate solution. The material retained its structure after the metal ion exchange and calcination.

^{29}Si MAS NMR spectra of each sample (Fig. 6) demonstrate a broad signal at −100 ppm and shoulders at −90, −107, and −110 ppm. According to Kolodziejski et al. [35], the main signal at −100 ppm is due to $Si(OSi)_3OH$ sites, whereas

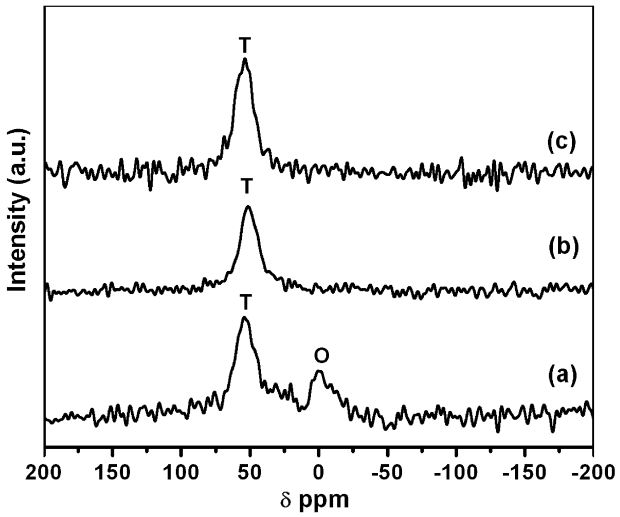

Fig. 5. ^{27}Al MAS NMR profile of (a) AlSBA-15 (10), (b) CuAlSBA-15 (10), (c) ZnAlSBA-15 (10). T = tetrahedral Al sites and O = octahedral Al sites.

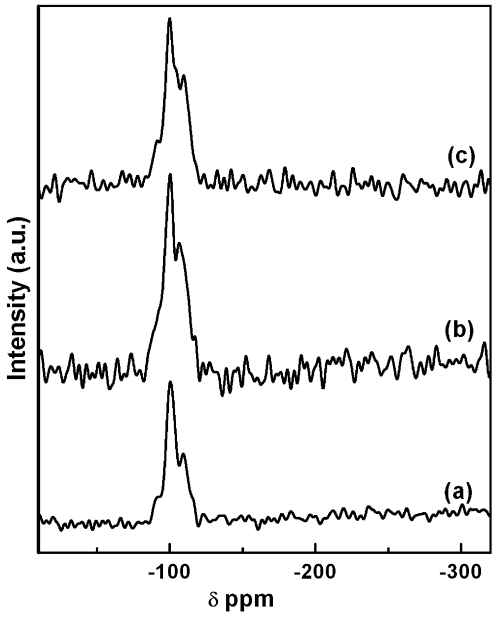

Fig. 6. ^{29}Si MAS NMR profile of (a) SBA-15, (b) AlSBA-15 (10), (c) CuAlSBA-15.

the shoulders at −90, −107, and −110 ppm are attributed to $Si(OSi)_2(OH)_2$, Si(3Si, 1Al), and $Si(OSi)_4$ structural units. There are no significant differences between ^{29}Si MAS NMR spectra of CuAlSBA-15, AlSBA-15, and SBA15.

3.1.5. Acidity measurements

Pyridine adsorption in situ FTIR spectroscopy was performed for AlSBA-15 and Cu-incorporated AlSBA-15 catalysts and the spectra recorded after outgassing at 200 °C are represented in Fig. 7. Adsorption of pyridine on the parent AlSBA-15 resulted in absorption bands at 1542 and 1451 cm^{-1}, which can be assigned to pyridine molecules interacting with Brönsted (B) and Lewis (L) acid sites, respectively. Incorporation of copper led to an increase in Lewis acidity. CuAlSBA-15 (10) catalysts prepared by exchanging with different copper acetate concen-

Table 2
Effect of copper acetate concentrations on Cu^{2+} exchange and their acidities

Catalyst	Copper acetate solution (mol/L)	Total exchange time (h)	Copper concentration (mmol/g)	Brönsted acidity I_{1542}	Lewis acidity I_{1451}	B/L I_{1542}/I_{1451}
AlSBA-15 (10)	–	–	–	2.23	2.44	0.91
CuAlSBA-15 (10)	0.01	18	0.14	1.68	3.23	0.52
CuAlSBA-15 (10)	0.03	18	0.21	1.05	5.01	0.21
CuAlSBA-15 (10)	0.06	18	0.26	1.14	4.56	0.25
CuAlSBA-15 (10)	0.1	18	0.33	1.56	3.47	0.45
CuSBA-15 (10)	0.03	40	0.40	0.79	3.91	0.20

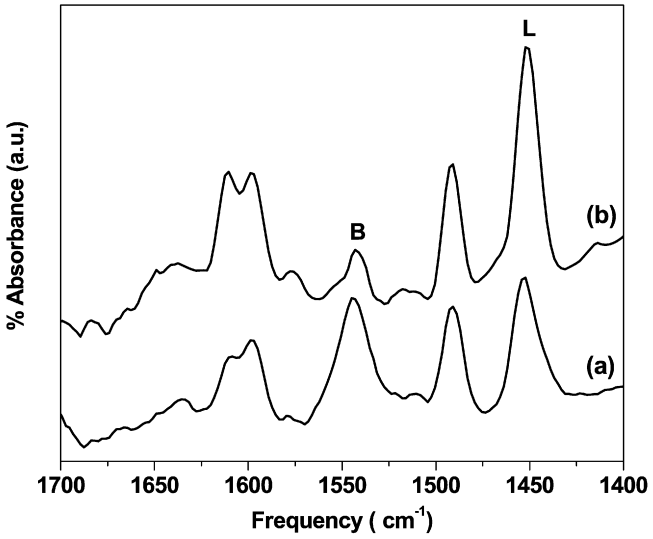

Fig. 7. FT-IR pyridine adsorption of (a) AlSBA-15 (10) and (b) CuAlSBA-15 (10) catalysts with Brönsted (B) and Lewis acid (L) peaks.

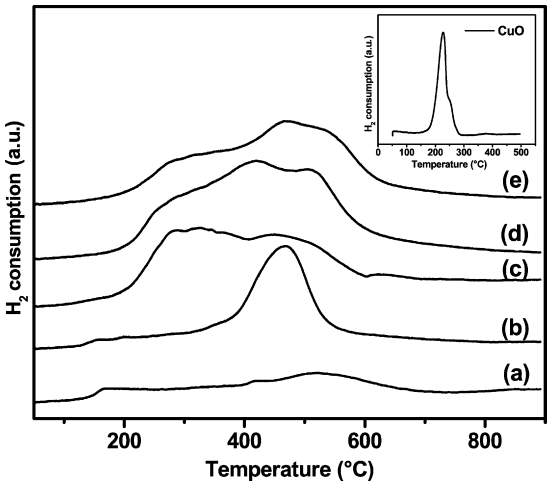

Fig. 8. H_2-TPR profiles of (a) CuO/SBA-15, (b) CuAlSBA-15 (40), (c) CuAlSBA-15 (30), (d) CuAlSBA-15 (20), (e) CuAlSBA-15 (10).

trations and the B/L ratios obtained by intensity measurements are listed in Table 2. It is seen that the B/L ratio increased as copper concentration increased in mesoporous support up to 0.21 mmol/g of Cu and then decreased thereafter. This suggests that optimum copper exchange occurs at lower concentrations of copper acetate (0.03 M). For overexchanged catalysts, the extra copper present in the catalysts is due to the formation of CuO clusters inside the pores and the catalyst surface [23].

3.1.6. TPR

H_2-TPR studies were performed for the identification of copper species in AlSBA-15 materials modified with copper. According to the literature [26,36,37] the following reduction processes can be considered:

$$CuO + H_2 \rightarrow Cu^0 + H_2O, \quad (1)$$

$$Cu^{2+} + 1/2H_2 \rightarrow Cu^+ + H^+, \quad (2)$$

$$Cu^+ + 1/2H_2 \rightarrow Cu^0 + H^+. \quad (3)$$

Reactions (1) and (2) occur at lower temperatures than reaction (3). TPR profiles of CuAlSBA-15 catalysts with different Si/Al ratios and CuO/SBA-15 are depicted in Fig. 8. The TPR graph of pure CuO shows a peak maximum at 207 °C (inset). The Cu^{2+}-exchanged AlSBA-15 samples show different peaks at 160–650 °C. The low-temperature peaks below 210 °C for copper-containing samples may be due to reduction of the copper–oxygen phase (not necessarily CuO) (reaction (1)). The peaks at >210 and >330 °C indicate the reduction of isolated Cu^{2+} cations in reactions (2) and (3), respectively. The results indicate that the copper ions are located mostly in extra-framework positions in the exchanged form. The different shoulders observed for these solids indicate that they contain Cu^{2+} species present in small clusters in different environments. It is also seen that as the Si/Al decreased, the temperature at the peak maximum of the first peak shifted to higher temperatures. The CuO/SBA-15 catalyst (Fig. 8a) showed a weak TPR profile, suggesting that it contains very-low-exchanged copper sites and that all of the isolated Cu^{2+} sites observed for CuAlSBA-15 catalysts are due to the exchange with the Brönsted acid sites in AlSBA-15 samples.

3.2. Hydroamination reaction

The hydroamination of phenylacetylene with 2,4-xylidine to give an enamine as an intermediate (not observed), which rearranges itself to form *N*-(1-phenylethylidene)-2,4-dimethylaniline (Scheme 1), was used as a model reaction for testing the catalytic activities of various catalysts. The reaction was highly selective, with only the preferred Markovnikov addition product observed. The different transition metal ions, such as Cu^{2+}, Zn^{2+}, Pd^{2+}, Co^{2+}, Mn^{2+}, La^{3+}, and Fe^{3+}, were exchanged with AlSBA-15 (10), and the catalytic activities in the hydroamination of PhAc with 2,4-xylidine were compared (Table 3). CuAlSBA-15 showed the highest activity, with 44 mol%

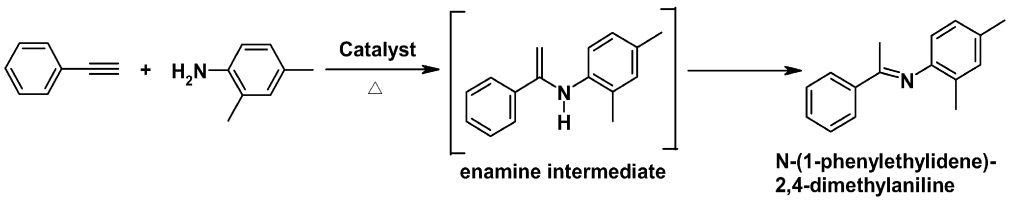

Scheme 1. Hydroamination of phenylacetylene with 2,4-xylidine.

Table 3
Catalytic activities of M^{n+}AlSBA-15 (10) in hydroamination of PhAc with 2,4-xylidine

M^{n+}	Cu^{2+}	Zn^{2+}	Pd^{2+}	Co^{2+}	Mn^{2+}	La^{3+}	Fe^{3+}	H^{+}
PhAc conversion (mol%)	44	31	10	5	4	7	4	4

Conditions: temperature = 110 °C, 2,4-xylidine to PhAc mole ratio = 2, catalyst wt = 0.1 g, total reactants wt = 2 g, time = 8 h.

conversion of PhAc after 4 h of reaction, with the others following in the decreasing order of CuAlSBA-15 > ZnAlSBA-15 > PdAlSBA-15 > LaAlSBA-15 > CoAlSBA-15 > MnAlSBA-15 > FeAlSBA-15.

As reported in the literature, the catalysts with Cu^{2+} and Zn^{2+} sites are highly active for hydroamination of alkynes by amines compared with other metal ions due to their moderately hard Lewis acidic properties [12,28]. Cu^{2+} ions exchanged with different supports, such as AlSBA-15, AlMCM-41, H-beta, and montmorillonite K-10, and the catalytic activities in the hydroamination of PhAc were compared (Table 1). The unexchanged catalysts (supports) showed very low catalytic activity. The turnover frequencies (TOF = mol of PhAc converted per mol of Cu^{2+} per hour) were the highest with CuAlSBA-15 (10) (TOF = 22) and CuAlMCM-41 (15) (TOF = 21) in the hydroamination of PhAc by 2,4-xylidine compared with clay- and zeolite-supported catalysts. The higher activities of the mesoporous-supported catalysts can be attributed to their higher surface areas and larger pore sizes.

Copper triflate was tested for its catalytic activity as the corresponding homogeneous counterpart by keeping the amount of copper the same as for CuAlSBA-15 (10). This catalyst was less active than CuAlSBA-15 (10) by ∼10%. This finding is contrary to the expectation that porous catalysts are often assumed to be less active than the corresponding homogeneous catalysts, because diffusion within the pores may slow the overall reaction. The higher activity of porous catalysts may be due to the presence of some Brönsted acid sites left unexchanged, which may act as promoters in hydroamination, which is absent in copper salts [38]. In contrast to the Cu^{2+} ion-exchanged materials, CuO showed no catalytic activity in the hydroamination reaction, which may be attributed to its basic nature. However, CuO/SBA-15 showed some activity (TOF = 3), possibly due to some exchangeable protons present in SBA-15. H_2-TPR results showed that the CuAlSBA-15 catalysts contained an insignificant amount of CuO, present mostly in the Cu^{2+} state, the active site for the hydroamination reaction in the present study.

Among the CuAlSBA-15 catalysts with different Si/Al ratios (as given in parentheses), the activity increased with decreasing Si/Al ratio (Table 1). Brönsted acidity increased with decreasing Si/Al ratio, which in turn increased the ion-exchange capacity and subsequently enhanced the number of exchanged Cu^{2+} ions. To determine the effect of Cu^{2+} concentration on catalytic activity, catalysts with different Cu^{2+} concentrations (0.14–0.40 mmol/g) were tested in the hydroamination of PhAc with 2,4-xylidine. The results, shown in Fig. 9, indicate that conversion of PhAc increased at copper concentrations up to 0.21 mmol/g and decreased at higher concentrations. These findings are in agreement with the acidity data given in Table 2. Brönsted acidity decreased with increasing Cu^{2+} concentration up to 0.21 mmol/g and then decreased with further increases. The nature of the copper species depends on the concentration of copper acetate solution as well as the time of exchange. Thus in overexchanged catalysts, copper oxide clusters may be formed inside the channels as well as on the surface, affecting the activity.

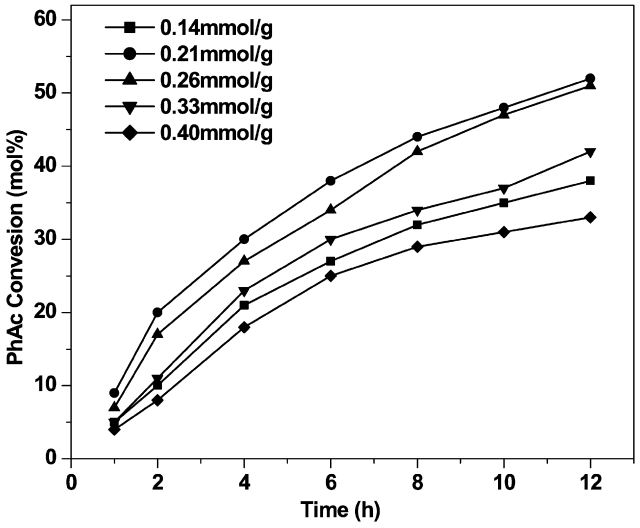

Fig. 9. Influence of Cu^{2+} concentration on catalytic activity conditions: catalyst = CuAlSBA-15 (10), temperature = 110 °C, 2,4-xylidine to PhAc mole ratio = 2, catalyst wt = 0.1 g, total reactants wt = 2 g.

CuAlSBA-15 (10) was used to study the effect of temperature (80–120 °C ranges) in the hydroamination of phenylacetylene with 2,4-xylidine. The results indicate that temperature has a remarkable effect on the conversion of PhAc (Fig. 10a). The conversion was only 10 mol% at 90 °C and increased to 52 mol% at 110 °C after 12 h. Following the initial rate approach, the graph of ln(rate) versus $1/T$ was plotted and from the slope of the straight line (slope $= -E_a/R$), the activation energy calculated was found to be 65 kJ/mol.

The effect of substrate concentrations on PhAc conversion was studied at 100 °C by keeping the total weight of the reaction

Table 4
Hydroamination of different alkynes and amines catalyzed by CuAlSBA-15

Entry[a]	Amine	Conversion (mol%)	Entry[b]	Alkynes	Conversion (mol%)
1	Aniline	61	1	1-Hexyne	15
2	*o*-Toluidine	38	2	1-Heptyne	31
3	*p*-Toluidine	52	3	3-Hexyne	NR
4	2,4-Xylidine	48	4	Phenylacetylene	61
5	2,4,6-Trimethylaniline	37	5	Diphenylacetylene	NR
6	2-Isopropylaniline	35	6	4-Ethynyltouene	52
7	4-Isopropylaniline	38	7	4-Ethynylanisole	55
8	4-Methoxyaniline	45	8	1-Ethynylnaphthalene	46
9	2-Chloroaniline	15			
10	4-Bromoaniline	21			
11	4-Nitroaniline	No reaction			
12	1-Naphthylamine	58			
13	*N*-Methylaniline	No reaction			
14	Cyclohexylamine	No reaction			

[a] Hydroamination of PhAc with amines. Conditions: catalyst = CuSBA-15 (10), amine to PhAc mole ratio = 2, toluene = 2 ml, temperature = 110 °C, catalyst wt = 0.15 g, total reactants wt = 2 g, time = 6 h, 100% selectivity for Markovnikov product.

[b] Hydroamination of alkynes with 2,4-xylidine. Conditions: catalyst = CuSBA-15 (10), 2,4-xylidine to alkyne mole ratio = 2, toluene = 2 ml, temperature = 110 °C, catalyst wt = 0.15 g, total reactants wt = 2 g, time = 6 h, NR = no reaction, 100% selectivity for Markovnikov product.

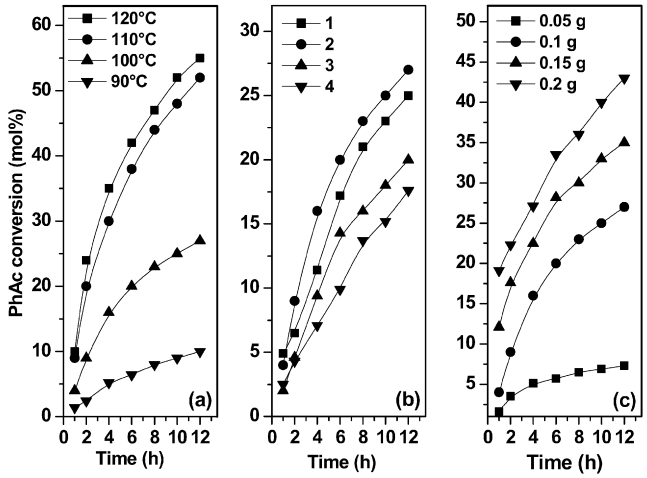

Fig. 10. (a) Effect of reaction temperature. Conditions: catalyst = CuAlSBA-15 (10), 2,4-xylidine to PhAc mole ratio = 2, catalyst wt = 0.1 g, total reactants wt = 2 g. (b) Effect of 2,4-xylidine to PhAc mole ratio. Conditions: catalyst = CuAlSBA-15 (10), temperature = 100 °C, catalyst wt = 0.1 g, total reactants wt = 2 g. (c) Effect of catalyst concentration. Conditions: catalyst = CuAlSBA-15 (10), temperature = 100 °C, 2,4-xylidine to PhAc mole ratio = 2, total reactants wt = 2 g.

mixture constant (Fig. 10b). As the molar ratio of 2,4-xylidine to PhAc was increased from 1 to 2, the PhAc conversion increased from 11 to 16% after 4 h. But further increases in the molar ratio of 2,4-xylidine to PhAc decreased the PhAc conversion. Higher PhAc conversions were observed at a 2,4-xylidine to PhAc molar ratio of 2.

The effect of catalyst concentration on PhAc conversion studied at 100 °C with a molar ratio of 2 (Fig. 10c) showed increasing PhAc conversion with increasing catalyst concentration. A linear increase in conversion occurred for up to 6 h, and the reaction slowed with only marginal increases at 6–12 h. At optimized reaction conditions (110 °C, 2,4-xylidine/PhAc 2, catalyst weight 0.15 g and total reactant weight 2 g with 2 ml of toluene as a solvent), PhAc conversion was 88 mol% after 20 h reaction.

To determine whether any active species of the catalyst are leaching into the reaction mixture, hydroamination of phenylacetylene with 2,4-xylidine to give an imine was carried out at optimized conditions with CuAlSBA-15 (10) catalyst. After 2 h (20 mol% conversion), the reaction was stopped and filtered hot, and then the reaction was continued with the filtrate under identical conditions. Conversion remained the same even after 20 h, indicating no leaching of any active species of the catalyst. The recyclability of CuAlSBA-15 catalyst was tested in the hydroamination of phenyl acetylene and 2,4-xylidine by conducting five runs (∼80 mol% conversion after 20 h) using optimized reaction conditions. After each run, the catalyst (brown in color) was repeatedly washed with toluene, dried at 120 °C for 2 h, and calcined at 500 °C in air for 4 h (turned white). It was then used in the hydroamination reaction with a fresh reaction mixture, and it was found that the conversion of PhAc was practically the same in all the five cycles.

To check the general applicability of the catalyst, two sets of reactions were carried out and the conversions were expressed as the conversion of alkyne. In the first set, different amines were reacted with phenyl acetylene (Table 4). The nature of substituents on the aromatic ring of aniline derivatives has significant effect over the reactivity. The electron-donating groups at the *-ortho* and *-para* positions gave higher conversions to yield the corresponding imines, which are comparable to that of aniline reaction. The sterically hindered amines, such as 2,4,6-trimethylaniline (37%) and 2-isopropylaniline (35%) and large-molecule 1-naphthylamine (58 mol%), gave higher conversions, which indicates that the bulky amines can easily pass through the mesopores of CuAlSBA-15. The amines with electron-withdrawing substituents, such as 2-chloroaniline (15%) and 4-bromoaniline (21%), were least reactive. No reactivity was observed when phenylacetylene was reacted with a secondary aromatic amine (*N*-methylaniline) and an aliphatic amine (cyclohexylamine), suggesting that CuAlSBA-15 is suitable only for aromatic primary amines for the hydroamination of alkynes.

In the second set, the reactions were carried out by reacting different alkynes with 2,4-xylidine (Table 4). Aromatic alkynes were more reactive than aliphatic alkynes, whereas terminal alkynes gave the higher yields. Internal alkynes (entries 3 and 5) did not undergo the reaction, indicating that this catalyst is suitable only for the hydroamination of terminal alkynes. The activated alkynes with electron-donating substituents, CH_3– and CH_3O–, gave better yields (entries 6 and 7), whereas the larger molecules, like 1-ethynylnaphthalene, showed high conversion (46%).

4. Conclusion

Cu^{2+} ion-exchanged AlSBA-15 catalysts were effectively used in intermolecular hydroamination of phenylacetylene with 2,4-xylidine. The state and behavior of copper in AlSBA-15 materials depend strongly on the method used for Cu inclusion. The reaction was catalyzed by Cu^{2+} ions obtained by exchanging with protons of AlSBA-15, not by the unexchanged copper present as its oxide. AlSBA-15 and AlMCM-41 were the best supports compared with zeolite beta and clay, whereas Cu- and Zn-exchanged AlSBA-15 catalysts showed higher activity compared with other metals. The alkynes and amines with electron-donating substituents showed higher activity, whereas the presence of electron-withdrawing groups on the aromatic ring retards the reaction. The catalyst did not catalyze hydroamination reactions involving internal alkynes, aromatic secondary amines, and aliphatic amines. These findings indicate that the CuAlSBA-15 catalyst is a versatile and reusable catalyst for intermolecular hydroamination of terminal alkynes with aromatic primary amines.

Acknowledgments

Support was provided by CSIR, New Delhi (a Senior Research Fellowship to G.V.S.) and DST, New Delhi.

References

[1] T.E. Müller, M. Beller, Chem. Rev. 98 (1998) 675.
[2] R.W. Layer, Chem. Rev. 63 (1963) 489.
[3] J.A. Loritsch, R.R. Vogt, J. Am. Chem. Soc. 61 (1939) 1462.
[4] J. Barluenga, F. Aznar, R. Liz, R. Rodes, J. Chem. Soc. Perkin Trans. 1 (1980) 2732.
[5] D. Tzalis, C. Koradin, P. Knochel, Tetrahedron Lett. 40 (1999) 6193.
[6] Y. Li, T.J. Marks, Organometallics 15 (1996) 3770.
[7] Y. Li, T.J. Marks, J. Am. Chem. Soc. 120 (1998) 1757.
[8] A. Haskel, T. Straub, M.S. Eisen, Organometallics 15 (1996) 3773.
[9] P.J. Walsh, A.M. Baranger, R.G. Bergman, J. Am. Chem. Soc. 114 (1992) 1708.
[10] F. Pohlki, S. Doye, Chem. Soc. Rev. 32 (2003) 104.
[11] J. Penzien, T.E. Muller, J.A. Lercher, Chem. Commun. (2000) 1753.
[12] J. Penzien, C. Haeßner, A. Jentys, K. Köhler, T.E. Müller, J. Lercher, J. Catal. 221 (2004) 302.
[13] J. Penzien, T.E. Muller, J.A. Lercher, Micropor. Mesopor. Mater. 48 (2001) 285.
[14] J. Penzien, R.Q. Su, T.E. Muller, J. Mol. Catal. A Chem. 182 (2002) 489.
[15] M.K. Richmond, S.L. Scott, H. Alper, J. Am. Chem. Soc. 123 (2001) 10521.
[16] S. Breitenlechner, M. Fleck, T.E. Müller, A. Suppan, J. Mol. Catal. A Chem. 214 (2004) 175.
[17] N. Lingaiah, N.S. Babu, K.M. Reddy, P.S.S. Prasad, I. Suryanarayana, Chem. Commun. (2007) 278.
[18] R. Ryoo, S. Jun, J.M. Kim, M.J. Kim, Chem. Commun. (1997) 2225.
[19] B.Z. Zhan, B. Moden, J. Dakka, J.G. Santiesteban, E. Iglesia, J. Catal. 245 (2007) 316.
[20] M.F. Ribeiro, J.M. Silva, S. Brimaud, A.P. Antunes, E.R. Silva, A. Fernandes, P. Magnoux, D.M. Murphy, Appl. Catal. B 70 (2007) 384.
[21] B.M. Choudary, M. Sateesh, M.L. Kantam, K.V.R. Prasad, Appl. Catal. A 171 (1998) 155.
[22] C.T. Abreu, M.F. Ribeiro, C. Henriques, G. Delahay, Appl. Catal. B 12 (1997) 249.
[23] V.A. Matyashak, A.N. Ilichev, A.A. Ukharsky, V.N. Korchak, J. Catal. 171 (1997) 245.
[24] H. Yahiro, M. Iwamoto, Appl. Catal. A 222 (2001) 163.
[25] V. Nieminen, N. Kumar, J. Datka, J. Paivarinta, M. Hotokka, E. Laine, T. Salmi, D.Y. Murzin, Micropor. Mesopor. Mater. 60 (2003) 159.
[26] I. Sobczak, M. Ziolek, M. Renn, P. Decyk, I. Nowak, M. Daturi, J. Lavalley, Micropor. Mesopor. Mater. 74 (2004) 23.
[27] Z. Luan, M. Hartmann, D. Zhao, W. Zhou, L. Kevan, Chem. Mater. 11 (1999) 1621.
[28] G.V. Shanbhag, S.B. Halligudi, J. Mol. Catal. A Chem. 222 (2004) 223.
[29] T. Joseph, G.V. Shanbhag, S.B. Halligudi, J. Mol. Catal. A Chem. 236 (2005) 139.
[30] G.V. Shanbhag, S.M. Kumbar, T. Joseph, S.B. Halligudi, Tetrahedron. Lett. 47 (2006) 141.
[31] D. Zhao, J. Feng, Q. Huo, N. Melosh, G.H. Fredrickson, B.F. Chmelka, G.D. Stucky, Science 279 (1998) 548.
[32] A. Bordoloi, B.M. Devassy, P.S. Niphadkar, P.N. Joshi, S.B. Halligudi, J. Mol. Catal. A 253 (2006) 239.
[33] E.P. Barrett, L.G. Joyner, P.P. Halenda, J. Am. Chem. Soc. 73 (1951) 373.
[34] R. Anwander, C. Palm, G. Gerstberger, O. Groeger, G. Engelhardt, Chem. Commun. (1998) 1811.
[35] W. Kolodziejski, A. Corma, M.T. Navarro, J. Perez-Periente, Solid State Nucl. Magn. Reson. 2 (1993) 253.
[36] T.F. Guidry, G.L. Price, J. Catal. 181 (1999) 16.
[37] C. Torre-Abreu, M.F. Ribeiro, C. Henriques, G. Delahay, Appl. Catal. B 12 (1997) 249.
[38] R.Q. Su, T.E. Muller, Tetrahedron 57 (2001) 6027.